

Graph Information Bottleneck for Remote Sensing Segmentation

Yuntao Shou, Wei Ai, Tao Meng

Abstract—Remote sensing segmentation has a wide range of applications in environmental protection, and urban change detection, etc. Despite the success of deep learning-based remote sensing segmentation methods (e.g., CNN and Transformer), they are not flexible enough to model irregular objects. In addition, existing graph contrastive learning methods usually adopt the way of maximizing mutual information to keep the node representations consistent between different graph views, which may cause the model to learn task-independent redundant information. To tackle the above problems, this paper treats images as graph structures and introduces a simple contrastive vision GNN (SC-ViG) architecture for remote sensing segmentation. Specifically, we construct a node-masked and edge-masked graph view to obtain an optimal graph structure representation, which can adaptively learn whether to mask nodes and edges. Furthermore, this paper innovatively introduces information bottleneck theory into graph contrastive learning to maximize task-related information while minimizing task-independent redundant information. Finally, we replace the convolutional module in UNet with the SC-ViG module to complete the segmentation and classification tasks of remote sensing images. Extensive experiments on publicly available real datasets demonstrate that our method outperforms state-of-the-art remote sensing image segmentation methods.

Index Terms—Remote Sensing Segmentation, Graph Learning, Contrastive Learning, Information Bottleneck.

I. INTRODUCTION

A. Motivation

REMOTE sensing segmentation has been widely developed in a variety of scenarios including land cover mapping, environmental protection, and road information extraction, which require high-quality feature representations to be learned from irregular objects (e.g., roads, trees, etc). In recent years, thanks to the powerful modeling ability for image data, convolutional neural network (CNN) and Transformer with attention module have provided an effective way to extract the underlying visual features and multi-scale features of images and exhibit guaranteed performance on remote sensing segmentation [1].

Although encouraging segmentation performance has been achieved, we argue that CNN-based and Transformer-based remote sensing segmentation models suffer from a limits. Taking Fig. 1 as an example, Fig. 1(a) shows the CNN-based image modeling method, which treats the image as a regular grid structure. Fig. 1(b) shows the Transformer-based image modeling method, which regards the image as a continuous

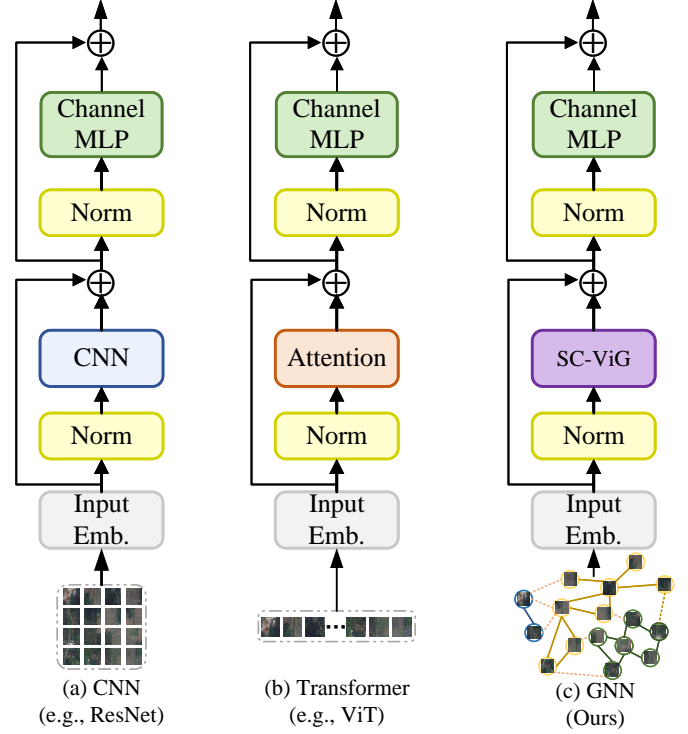


Fig. 1. Illustrative examples of different modeling approaches for an image. (a) CNNs view images as regular grid structures (i.e., squares and rectangles). (b) Transformer treats images as a continuous sequence structure. (c) We believe that both sequence structure and grid structure are special cases of graph structures, and graph structure can flexibly model regular and irregular objects. We thus view images as graph structures.

sequence structure. Both of the above methods are unable to model irregular objects. As shown in Figure 1(c), we argue that both grid and sequence structures are special cases of graph structures, and that GNN-based approaches [2], [3], [4], [5], [6] are capable of modeling data in non-Euclidean spaces. Therefore, we propose a GNN-based remote sensing image modeling method for multi-scale feature extraction of irregular objects.

Recent advances in graph contrastive representation learning have demonstrated that it can improve model convergence and improve model robustness. Nevertheless, the existing methods suffer from two limitations. First, most existing methods perform feature augmentation by randomly masking graph views to obtain better node representations. However, randomly masking nodes and edges may be too random, which destroys the expressive ability of the semantic information of the original graph. Second, most existing methods gen-

Corresponding Author: Tao Meng (mengtao@hnan.edu.cn)

Y. Shou, W. Ai, and T. Meng are with School of computer and Information Engineering, Central South University of Forestry and Technology, Hunan 410004, China. (shouyuntao@stu.xjtu.edu.cn, aiwei@hnu.edu.cn, mengtao@hnu.edu.cn)

erate multiple graph contrastive views and obtain consistent node representations by maximizing the mutual information between them, which may force the model to learn task-independent semantic information. We argue that a good feature augmentation method should minimize task-independent redundant information.

To address the aforementioned issue, we propose a simple contrastive vision GNN (SC-ViG) architecture for remote sensing segmentation, which consists of key steps, i.e., an adaptive feature augmentation module and a graph contrastive learning via information bottleneck module.

First, we introduce a learnable graph contrastive view to adaptively learn whether to mask nodes and edges to improve the node representation ability of the original graph, which is optimized together with downstream remote sensing segmentation and classification in an end-to-end learning manner. The intuition behind adaptive masking is to randomly mask nodes and edges without a policy regardless of the degree of the corresponding nodes. However, GCNs aggregate the information of surrounding neighbor nodes through the message passing mechanism, which makes it easy for GCNs to reconstruct the feature information of popular nodes, but it is difficult to reconstruct the feature information of isolated nodes with low degrees. These adaptive masking generated graph contrastive view increases the ability against imbalanced learning for remote sensing segmentation.

Second, we propose to integrate different graph-contrastive views into compact representations for downstream remote sensing segmentation tasks, which can further improve the feature representation capabilities of nodes. Recent advances have shown that downstream performance can be improved by fusing complementary semantic information between different views. Therefore, we argue that maximizing the mutual information (MI) between graph contrastive views forces a consistent representation of the graph structure, which leads the model to capture task-independent redundant information. Inspired by the information bottleneck (IB) theory, we use it to minimize the MI between the original graph and the generated contrastive view while preserving task-relevant semantic information. Through the above approach, the model can jointly learn complementary semantic information between different views.

B. Our Contributions

Compared with previous work, the contributions of this paper are summarized as follows.

- 1) We propose a simple contrastive vision GNN (SC-ViG) architecture for remote sensing segmentation, which enables flexible modeling of irregular objects
- 2) We introduce a novel graph contrastive learning approach to optimize node representations by adaptively masking nodes and edges, which improves the representation ability of graph structure.
- 3) We innovatively embed the information bottleneck theory into the graph contrastive learning method, which can effectively eliminate redundant information while preserving task-related information.

- 4) Extensive experiments demonstrate that our method outperforms the state-of-the-art on three publicly available datasets.

II. RELATED WORK

A. CNN, and Transformer for Remote Sensing Segmentation

The early mainstream network architecture for remote sensing segmentation extracts visual features of images by using CNN. The earliest remote sensing image segmentation methods based on CNN are all evolved from FCN ([7], [8], etc) and UNet (e.g., [9], [10], etc). UNet extracts the context and location information of the image by designing a U-shaped structure based on the encoder and decoder, where both of them are composed of convolutional layers, skip connections, and pooling layers. FCN extracts image features through several convolutional layers and then connects a deconvolutional layer to obtain a feature map of the same size as the raw image, so as to predict the image pixel by pixel. However, both FCN and UNet algorithms need to down-sample to continuously expand the receptive field when extracting image features, which leads to the loss of image position information. To alleviate the problem of information loss caused by the downsampling operation, the DeepLab series [11], uses hole convolution to increase the receptive field to obtain multi-scale feature information. The HRNet proposed by Wang et al. [12] achieves high-resolution semantic segmentation by extracting feature maps of different resolutions and recovering high-resolution feature maps.

Transformer [13] is widely used in the image processing field because of its powerful global information processing capabilities. ViT proposed by Dosovitskiy et al. [14] applied the Transformer architecture to CV for the first time, and she used the attention to extract global visual features. Since the complexity of the attention is $O(n^2)$, this leads to a very large number of parameters in the model, and the model is difficult to train. To solve the above problems, Liu et al. [15] proposed Swin-Transformer, which improves the problem of high model complexity through a hierarchical attention mechanism. The Wide-Context Transformer proposed by Ding et al. [16] extracts global context information by introducing a Context Transformer while using CNN to extract features. Zhang et al. [17] extract multi-scale contextual features by combining Swin-Transformer and dilated convolutions, and use a U-shaped decoder to achieve image semantic segmentation.

B. Graph Neural Networks

Kipf et al. [18] were the first to propose graph convolutional neural networks. In recent years, spatial-based GCNs and spectral-based GCNs have started to receive widespread attention, and they are applied to graph-structured data (e.g., social networks [19] and citation networks [20], etc.).

In recent years, graph neural network (GNN) has received extensive attention from researchers due to its powerful feature extraction capabilities, and it has been widely used in action recognition [21], point cloud analysis [22] and other fields [23]. GNN can flexibly model irregular objects and extract global location feature information. In the remote sensing

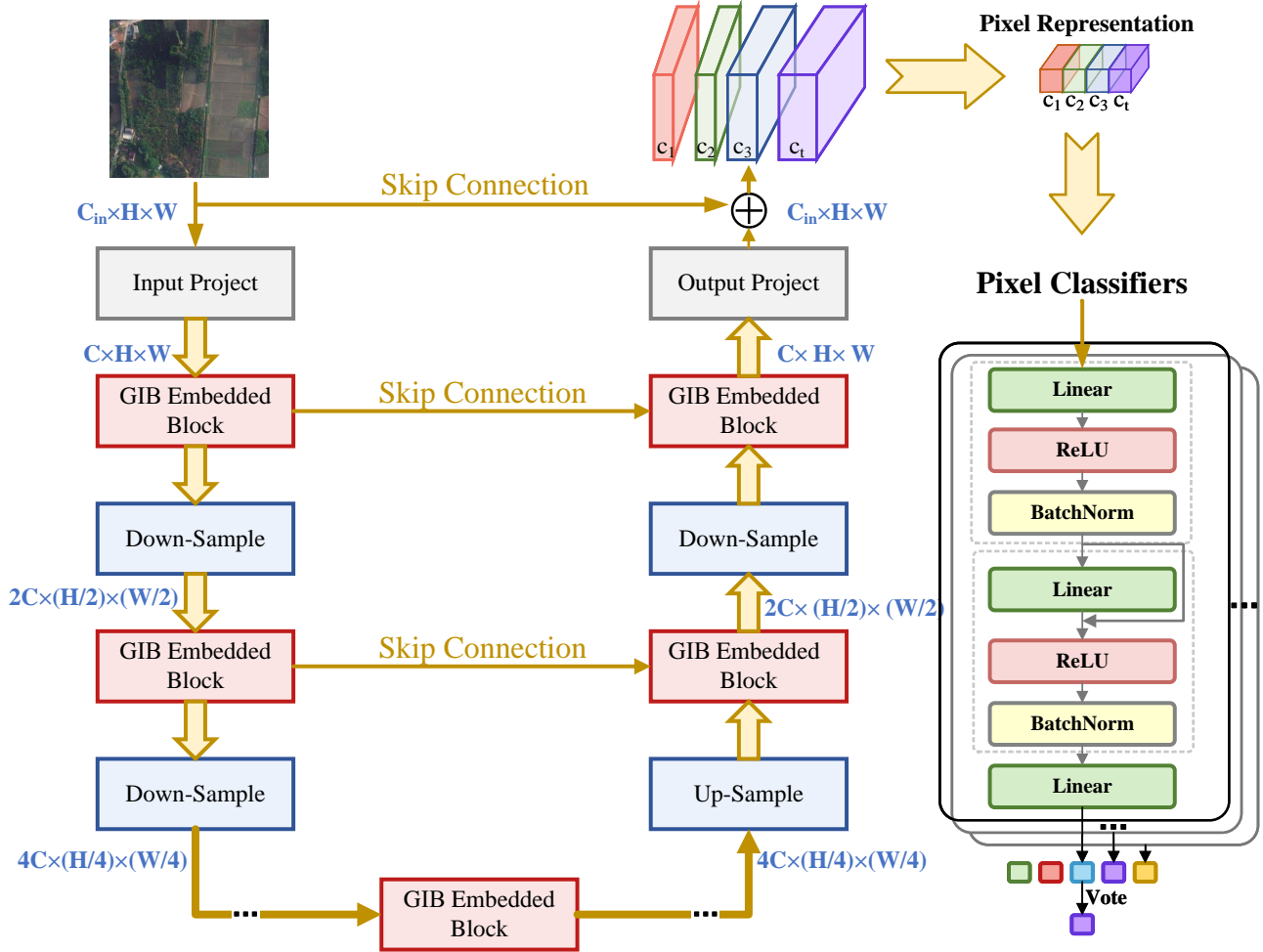


Fig. 2. The architecture of the proposed GraphUNet method. Specifically, we first divide the image into patches and construct it as a graph. Then we replace the convolutional block in UNet with our GCN Block and use the constructed graph as the input. Finally, we build a MLP to classify pixels.

segmentation field, Saha et al. [24] use GNN to aggregate and label unlabeled data to improve the ability of the model to approach the target domain.

C. Graph Contrastive Learning

Graph contrastive learning (GCL) aims to learn compact representations of nodes or subgraphs in graph data, emphasizing similarities within the same graph and differences between different graphs. GCL has been applied in many fields, including social network analysis, drug discovery, image analysis, etc. For example, in social networks, similarities between users can be discovered through GCL, and in drug discovery, potential drug similarities can be mined by contrasting molecular structures.

In recent research, DGI [25] and InfoGraph [26] obtain compact representations of graphs or nodes by maximizing the mutual information (MI) between different augmented views. MVGRL [27] argues that it can achieve optimal feature representation by contrasting first-order neighbor nodes and performing node diffusion to maximize the MI between subgraphs. GraphCL [28] constructs four types of augmented

views and maximizes the MI between them. GraphCL enables better generalization performance on downstream tasks. However, GraphCL requires complex manual feature extraction. We argue that a good contrast-augmented view should be structurally heterogeneous while semantically similar, while previous research work maximizes the mutual information between nodes, which may lead to overfitting of the model.

III. APPROACH

In this section, we illustrate the construction of graph-structured data from images, and introduce the GCL architecture with the information bottleneck to learn to extract global information locations of images.

A. Structure Flow

Our main goal is to design an efficient modeling paradigm for global location information extraction of irregular objects, detailed in Fig. 2. For a given remote sensing image ($H \times W \times 3$), we first divide it into M patches. Then we map each image patch to a D -dimensional feature space

$x_i \in \mathbb{R}^D$, and obtain the feature vector X . We consider X to be a node in the graph, i.e., $V = \{v_1, v_2, \dots, v_N\}$. For node v_i , we use the KNN algorithm to find its K neighbors $N(v_i) = \{v_i^1, v_i^2, \dots, v_i^K\}$. For $v_j \in N(v_i)$, we connect an edge e_{ji} from v_j to v_i . Through the above process, we get a directed graph $G = (V, E)$. Follow UNet's network architecture design, feature embedding for images uses N encoders for feature encoding. Each stage consists of a GIB Embedding block (GE), a skip connection module and a downsampling layer. GE Block utilizes the inherent flexible modeling of non-Euclidean distance in the graph structure, follows the global modeling rules of node aggregation, and customizes the global position information interaction of the image. We downsample the feature maps with a 3×3 kernel. Similarly, the decoder stage consists of the proposed GE block and an upsampling layer to decode and reconstruct features. To ensure the effective utilization of information and the depth of network training, the decoder input of each stage is connected with the output of the encoder of the same stage. Finally, a convolutional layer is applied to generate the segmented image $S \in C_{in} \times H \times W$, which is predicted pixel by pixel.

B. GCN Embedded Block

The advantages of using a graph structure to model images are as follows: 1) The graph can flexibly handle data with non-Euclidean distances. 2) Compared with regular grid or sequence structures, graphs can model irregular objects while eliminating redundant information, and remote sensing images are mostly irregular objects. 3) The graph structure establishes the connection between objects (e.g., roads, trees, etc) through the connection between nodes and edges.

Specifically, for an input image feature X , we first construct a directed graph $G = G(x)$. To obtain the global location information of the image and update node features, we use graph convolution operations to aggregate and update node features. The formula is defined as follows:

$$\begin{aligned} G' &= F(G, W) \\ &= \text{Update}(\text{Aggregate}(G, W_{\text{agg}}), W_{\text{update}}) \\ &= \text{LeakyReLU} \left(\sum_{r \in \mathcal{R}} \sum_{j \in \mathcal{N}_i^r} \frac{1}{|\mathcal{N}_i^r|} \left(\omega_{ij}^{(l)} W_{\theta_1}^{(l)} x_j^{(l)} \right. \right. \\ &\quad \left. \left. + \omega_{ii}^{(l)} W_{\theta_2}^{(l)} x_i^{(l)} \right) \right) \end{aligned} \quad (1)$$

where W_{agg} , W_{update} , $W_{\theta_1}^{(l)}$, $W_{\theta_2}^{(l)}$ is learnable weights, w_{ij} is the edge weight between node i and node j , and its formula is defined as follows:

$$\begin{aligned} \omega_{ij}^{(l+1)} &= \text{softmax} \left(W^{(l)} [x_i^{(l)} \oplus x_j^{(l)}] \right) \\ &= \frac{\exp \left[x_i^{(l)} \oplus x_j^{(l)} \right]}{\sum_{\eta \in \mathcal{N}_i} \exp \left[x_i^{(l)} \oplus x_j^{(l)} \right]}, \end{aligned} \quad (2)$$

To capture the location information of key regions in the image, we further introduce a multi-head attention mechanism to update node features. The format is defined as follows:

$$\mathbf{x}'_i = [\text{head}^1 W_{\text{update}}^1, \text{head}^2 W_{\text{update}}^2, \dots, \text{head}^h W_{\text{update}}^h] \quad (3)$$

where h represents the number of multi heads, we set $h = 4$.

We introduce the residual idea, and project node features to the same domain through a linear layer, which can help restore structural features and global position information. In addition, we also insert the LeakyReLU non-activation function to improve the nonlinear fitting ability of the model. The formula is expressed as follows:

$$Y = \text{LeakyReLU}(\text{GraphConv}(XW_{\text{in}})) W_{\text{out}} + X \quad (4)$$

To improve the feature transformation ability of nodes and alleviate the over-smoothing phenomenon of GCN, we use feed-forward network (FFN) to perform feature mapping on each node again. The formula of FFN is defined as follows:

$$Y' = \text{LeakyReLU}(YW_1) W_2 + Y \quad (5)$$

where W_1 and W_2 are the learnable parameters.

C. Graph Information Bottleneck

The principle of graph information bottleneck (GIB) is to introduce information bottleneck (IB) on the basis of GCL to perform contrastive learning between nodes or graphs. It forces the node representation Z_X to minimize the task-irrelevant information \mathcal{D} and maximize the information Y relevant to the downstream tasks.

Specifically, we follow the local dependency assumption for graph-structured data: for a given node v , node v 's first-order neighbor node data are related to node v , while the rest of the graph's data are independent and identically distributed with node v . The hypothesis space represented by nodes can be constrained according to local dependency assumptions, which reduces the difficulty of GIB optimization. We assume that $\mathbb{P}(Z_X | \mathcal{D})$ represents modeling the correlation between node features hierarchically. In each iteration l , the representation of each node is optimized by aggregating surrounding neighbor node information and graph structure information $Z_A^{(l)}$. Therefore, the optimization goal of GIB is defined as follows:

$$\begin{aligned} &\min_{\mathbb{P}(Z_X^{(L)} | \mathcal{D}) \in \Omega} \text{GIB}_\beta(\mathcal{D}, Y; Z_X^{(L)}) \\ &\triangleq \left[-I(Y; Z_X^{(L)}) + \beta I(\mathcal{D}; Z_X^{(L)}) \right] \end{aligned} \quad (6)$$

where Ω conforms to the representation space of Markov chain probability dependence within a given data set \mathcal{D} , $I(\cdot, \cdot)$ represents mutual information between feature vectors, $Z_X^{(L)}$ represents the feature representations of the nodes, and β is the balance coefficient. In Eq. 6, the model only needs to optimize two distributions, i.e., $\mathbb{P}(Z_A^{(l)} | Z_X^{(l-1)}, A)$, and $\mathbb{P}(Z_X^{(l)} | Z_X^{(l-1)}, Z_A^{(l)})$, where $Z_A^{(l)}$ is the graph structure information.

However, in Eq. 6, calculating the mutual information $I(Y; Z_X^{(L)})$ and $I(\mathcal{D}; Z_X^{(L)})$ is a difficult estimation problem. Therefore, we follow the IB criterion to introduce variational bounds on $I(Y; Z_X^{(L)})$ and $I(\mathcal{D}; Z_X^{(L)})$ to effectively perform parameter optimization. We give the upper and lower bounds

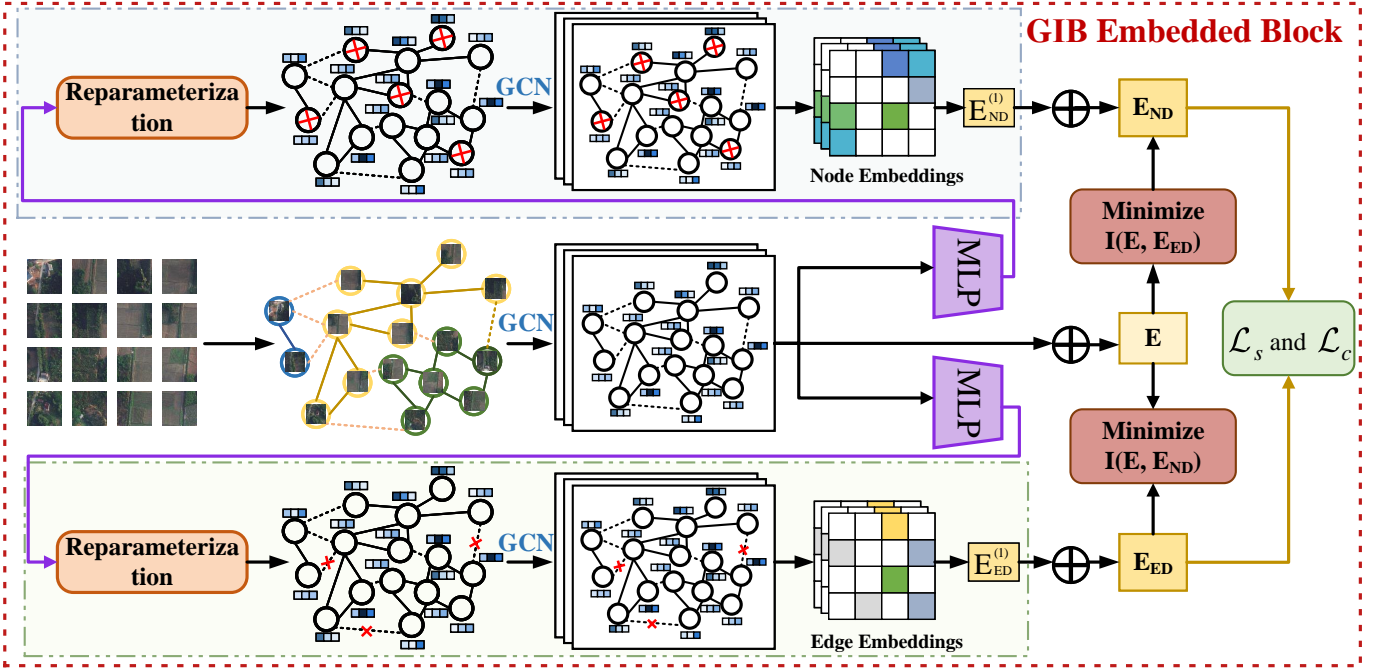


Fig. 3. The overview the GCN Embedded Block framework. We synthesize node-mask and edge-mask views to obtain better node representations. Specifically, we introduce information bottleneck theory in multiple graph comparison views to maximize feature information related to node classification tasks while minimizing redundant information of nodes.

of $I(\mathcal{D}; Z_X^{(L)})$ and $I(Y; Z_X^{(L)})$ as shown in Theorems 1 and 2 respectively.

Theorem 1. For any class distribution given $\mathbb{Q}_1(Y_v|Z_{X,v}^{(L)})$ for $v \in V$ and $\mathbb{Q}_2(Y)$ in a graph, we can obtain a theoretical lower bound for $I(Y; Z_X^{(L)})$:

$$I(Y; Z_X^{(L)}) \geq 1 + \mathbb{E} \left[\log \frac{\prod_{v \in V} \mathbb{Q}_1(Y_v|Z_{X,v}^{(L)})}{\mathbb{Q}_2(Y)} \right] + \mathbb{E}_{\mathbb{P}(Y)\mathbb{P}(Z_X^{(L)})} \left[\frac{\prod_{v \in V} \mathbb{Q}_1(Y_v|Z_{X,v}^{(L)})}{\mathbb{Q}_2(Y)} \right] \quad (7)$$

Theorem 2. For any given node feature distribution $\mathbb{Q}(Z_X^{(l)})$ and graph structure information distribution $\mathbb{Q}(Z_A^{(l)})$, we use Markov chain dependence to get the upper bound of $I(Y; Z_X^{(L)})$ as follows:

$$I(\mathcal{D}; Z_X^{(L)}) \leq I(\mathcal{D}; \{Z_X^{(l)}\}_{l \in S_X} \cup \{Z_A^{(l)}\}_{l \in S_A}) \leq \sum_{l \in S_A} \text{AIB}^{(l)} + \sum_{l \in S_X} \text{XIB}^{(l)} \quad (8)$$

where $l \in \{S_X, S_A\}$, and

$$\text{AIB}^{(l)} = \mathbb{E} \left[\log \frac{\mathbb{P}(Z_A^{(l)}|A, Z_X^{(l-1)})}{\mathbb{Q}(Z_A^{(l)})} \right], \quad \text{XIB}^{(l)} = \mathbb{E} \left[\log \frac{\mathbb{P}(Z_X^{(l)}|Z_X^{(l-1)}, Z_A^{(l)})}{\mathbb{Q}(Z_X^{(l)})} \right] \quad (9)$$

where AIB and XIB represents the adjacency matrix features and the node features obtained using the IB criterion, respectively.

To use GIB, we optimize $\mathbb{P}(Z_A^{(l)}|Z_X^{(l-1)}, A)$ and $\mathbb{P}(Z_X^{(l)}|Z_X^{(l-1)}, Z_A^{(l)})$ given a theoretical upper and lower bound. Next, we will specify the optimization goals of GIB.

Objective for training. To update model parameters in GIB, we need to calculate the theoretical boundary of GIB in 6. Specifically, we use a uniform distribution to optimize the classification problem: $Z_A \sim \mathbb{Q}(Z_A)$, $Z_{A,v} = \cup_{t=1}^T \{u \in V_{vt} | u \stackrel{\text{iid}}{\sim} \text{Cat}(\frac{1}{|V_{vt}|})\}$. Therefore, we can obtain an estimate of $\text{AIB}^{(l)}$ as follows:

$$\widehat{\text{AIB}}^{(l)} = \mathbb{E}_{\mathbb{P}(Z_A^{(l)}|A, Z_X^{(l-1)})} \left[\log \frac{\mathbb{P}(Z_A^{(l)}|A, Z_X^{(l-1)})}{\mathbb{Q}(Z_A^{(l)})} \right] \quad (10)$$

$\text{AIB}^{(l)}$ can be formally defined as follows:

$$\widehat{\text{AIB}}_C^{(l)} = \sum_{v \in V, t \in [T]} \text{KL}(\text{Cat}(\phi_{vt}^{(l)}) || \text{Cat}(\frac{1}{|V_{vt}|})) \quad (11)$$

For the estimation of XIB, we use a learnable Gaussian distribution to set $\mathbb{Q}(Z_X^{(l)})$. Specifically, for a given node v , $Z_X \sim \mathbb{Q}(Z_X)$, we assume $Z_{X,v} \sim \sum_{i=1}^m w_i \text{Gaussian}(\mu_{0,i}, \sigma_{0,i}^2)$.

Therefore $\widehat{\text{XIB}}^{(l)}$ is formally defined as follows:

$$\widehat{\text{XIB}}^{(l)} = \log \frac{\mathbb{P}(Z_X^{(l)}|Z_X^{(l-1)}, Z_A^{(l)})}{\mathbb{Q}(Z_X^{(l)})} = \sum_{v \in V} \left[\log \Phi(Z_{X,v}^{(l)}; \mu_v, \sigma_v^2) - \log \left(\sum_{i=1}^m w_i \Phi(Z_{X,v}^{(l)}; \mu_{0,i}, \sigma_{0,i}^2) \right) \right] \quad (12)$$

where $\mu_{0,i}, \sigma_{0,i}, w_i$ are the learnable.

Combining Eqs. 11 and 12, we can estimate $I(\mathcal{D}; Z_X^{(L)})$ as follows:

$$I(\mathcal{D}; Z_X^{(L)}) \rightarrow \sum_{l \in S_A} \widehat{\text{AIB}}^{(l)} + \sum_{l \in S_X} \widehat{\text{XIB}}^{(l)} \quad (13)$$

We use cross entropy to estimate $I(Y; Z_X^{(L)})$ as follows:

$$I(Y; Z_X^{(L)}) \rightarrow - \sum_{v \in V} \text{Cross-Entropy}(Z_{X,v}^{(L)} W_{\text{out}}; Y_v) \quad (14)$$

By combining Eqs. 13 and 14, we can get the optimization objective of GIB.

D. Instantiating GIB-RSS

After detailing the optimization principles of GIB, we will explain the GIB-RSS architecture we designed as shown in Fig. 3.

Node-Masking View. To improve the feature representation ability of nodes in the learning process, we perform learnable node masking before each information aggregation and feature update of GCN. The formula for the node mask view we created is as follows:

$$\mathcal{G}_{ND}^{(l)} = \left\{ \left\{ v_i \odot \eta_i^{(l)} \mid v_i \in \mathcal{V} \right\}, \mathcal{E}, \mathcal{R}, \mathcal{W} \right\}, \quad (15)$$

where $\eta_i^{(l)} \in \{0, 1\}$ is sampled from a parameterized Bernoulli distribution $Bern(\omega_i^l)$, and $\eta_i^{(l)} = 0$ represents masking node v_i , $\eta_i^{(l)} = 1$ represents keeping node v_i .

Edge-masking View. The goal of the edge-masking view is to generate an optimized graph structure, and the formula is defined as follows:

$$\mathcal{G}_{ED}^{(l)} = \left\{ \mathcal{V}, \left\{ e_{ij} \odot \eta_{ij}^{(l)} \mid e_{ij} \in \mathcal{E}, \mathcal{R}, \mathcal{W} \right\} \right\}, \quad (16)$$

where $\eta_{ij}^{(l)} \in \{0, 1\}$ is also sampled from a parameterized Bernoulli distribution $Bern(\omega_{ij}^l)$, and $\eta_{ij}^{(l)} = 0$ represents perturbing edges e_{ij} , $\eta_{ij}^{(l)} = 1$ represents keeping edge e_{ij} .

After obtaining the masked node and edge-masking views, we input them into GCN for feature representation to obtain optimized multi-views. The formula is defined as follows:

$$\begin{aligned} \mathbf{E}_{ND}^{(l)} &= \text{GraphConv} \left(\mathbf{E}_{ND}^{(l-1)}, \mathcal{G}_{ND}^{(l)} \right), \\ \mathbf{E}_{ED}^{(l)} &= \text{GraphConv} \left(\mathbf{E}_{ED}^{(l-1)}, \mathcal{G}_{ED}^{(l)} \right). \end{aligned} \quad (17)$$

where GraphConv represents the graph convolution operation, and we choose GAT as our graph encoder. \mathbf{E}_{ND} and \mathbf{E}_{ED} represent the node feature representations of node-masking view and edge-masking view respectively, \mathbf{G}_{ND} and \mathbf{G}_{ED} represent node-masking view and edge-masking view respectively.

After obtaining the node mask and edge mask views, we combine Eqs. 13 and 14 to jointly optimize the self-supervised losses \mathcal{L}_s and \mathcal{L}_c as follows:

$$\begin{aligned} \min(\mathcal{L}_s + \mathcal{L}_c) &= I(\mathcal{D}^{(ED)}; Z_X^{(ED)}) + I(Y; Z_X^{(ED)}) \\ &+ I(\mathcal{D}^{(ND)}; Z_X^{(ND)}) + I(Y; Z_X^{(ND)}) \end{aligned} \quad (18)$$

where $\mathcal{D}^{(ED)}$ and $\mathcal{D}^{(ND)}$ represent the graph structure of the node-masking and edge-masking views respectively, and $Z_X^{(ED)}$ and $Z_X^{(ND)}$ represent the node features of the node-masking and edge-masking views respectively.

E. Model Training

The cross-entropy loss function is used to measure the difference between the probability distribution of the model output and the distribution of the actual labels, thereby guiding the model to optimize parameters.

$$\mathcal{L} = - \frac{1}{\sum_{s=1}^N c(s)} \sum_{i=1}^N \sum_{j=1}^{c(i)} \log \mathcal{P}_{i,j}[y_{i,j}] + \lambda \|\theta\|_2 \quad (19)$$

where N represents the number of remote sensing images used for training, $c(i)$ represents the number of objects to be segmented in sample i , $\mathcal{P}[i,j]$ is the label probability distribution of object j in sample i , $y_{i,j}$ is the prediction label of object j in sample i , λ is the weight attenuation coefficient, and θ is the trainable network parameter.

IV. EXPERIMENTS

In this section, we verify the effectiveness of the proposed GraphUNet on remote sensing image segmentation tasks.

A. Benchmark Datasets Used

For the GraphUNet model, we use the widely used datasets UAVid [29], Vaihingen [30] and Potsdam [31] datasets for experimental evaluation. The UAVid dataset comes with two spatial resolutions. Specifically, the UAVid dataset contains a total of 420 images, and each image is cropped to a size of 1024×1024 . The Vaihingen dataset consists of 33 images with a spatial resolution of 2494×2064 . Each image is cropped to 1024×1024 . The Potsdam dataset contains 38 image patches with a spatial resolution of 6000×6000 , and we crop the original image size to 1024×1024 . The LoveDA dataset contains 5, 987 high-resolution remote sensing images with size 1024×1024 , 2, 522 images are used for training, 1, 669 images are used for validation, and 1, 796 images are used for testing. The data information of the dataset is shown in Table I.

TABLE I
THE DIVISION OF THE TRAIN SET, VAL SET AND TEST SET IN THE BENCHMARK DATASET AND THE RESOLUTION INFORMATION OF THE IMAGE.

Datasets	Resolutions	Train	Test	Val
UAVid	$3840 \times 2160/4096 \times 2160$	200	150	70
Vaihingen	2494×2064	15	17	1
Potsdam	6000×6000	22	14	1
LoveDA	1024×1024	2,522	1,796	1,669

B. Experimental Settings

GraphUNet is implemented on NVIDIA A100 GPU with 80G memory using PyTorch framework. For the hyperparameters in the experiments, the paper utilize the AdamW optimizer for gradient updates. The GraphUNet's learning rate (LR) is set to $5e-4$ and a cosine learning rate decay is utilized to

TABLE II

EXPERIMENTAL RESULTS OF OUR METHOD AND SOTA METHODS ON THE UAVID DATASET. THE OPTIMAL VALUES IN COLUMNS ARE SHOWN IN BOLD.

Methods	Backbone	Clutter	Building	Road	Tree	Vegetation	MovingCar	StaticCar	Human	mIoU
MSD	-	56.8	79.6	73.9	73.9	56.1	63.2	31.8	20.0	56.9
CANet	-	65.8	87.0	61.9	78.8	77.9	48.0	68.5	20.0	63.5
DANet	ResNet	65.1	86.2	78.0	77.9	60.9	60.0	47.1	8.9	60.5
SwiftNet	ResNet	63.9	84.9	61.3	78.3	76.4	51.2	62.4	15.8	61.8
BiSeNet	ResNet	64.5	85.8	61.0	78.1	77.1	48.8	63.2	17.4	62.0
MANet	ResNet	64.4	85.1	77.9	77.4	60.5	67.5	53.4	14.6	62.6
ABCNet	ResNet	67.3	86.1	81.5	79.7	63.3	69.2	48.3	13.6	63.6
Segmenter	ViT-Tiny	63.7	85.2	80.1	77.0	58.1	58.4	35.3	13.9	59.0
SegFormer	MiT-B1	67.3	87.3	79.8	80.1	62.7	71.7	52.7	29.3	66.3
BANet	ResT-Lite	65.9	86.0	81.2	79.1	61.9	68.7	52.4	20.5	64.4
BoTNet	ResNet	65.4	85.1	79.1	78.4	61.2	66.3	52.0	23.1	63.8
CoaT	CoaT-Mini	68.9	89.1	79.8	80.4	61.7	69.5	60.2	19.1	66.1
UNetFormer	ResNet	67.7	86.4	82.0	81.2	64.1	74.0	55.8	30.9	67.8
GIB-RSS	-	71.2	89.0	83.0	81.9	79.7	70.6	59.3	29.9	70.6

TABLE III

EXPERIMENTAL RESULTS OF OUR METHOD AND SOTA LIGHTWEIGHT METHODS ON THE VAIHINGEN DATASET. THE OPTIMAL VALUES IN COLUMNS ARE SHOWN IN BOLD.

Methods	Backbone	Imp.suf.	Building	Lowveg.	Tree	Car	MeanF1	OA	mIoU
DABNet	-	88.0	89.1	73.9	85.0	59.9	79.2	83.9	69.9
ERFNet	-	88.7	89.8	76.2	86.1	54.0	79.0	86.2	70.3
BiSeNet	ResNet	88.7	90.7	81.0	87.1	72.9	84.1	86.6	76.3
PSPNet	ResNet	88.8	92.9	81.8	88.1	44.2	79.2	88.0	76.1
DANet	ResNet	89.7	94.1	81.9	86.9	44.6	79.4	87.6	69.6
FANet	ResNet	91.2	94.1	83.1	88.7	72.0	85.8	90.0	76.0
EaNet	ResNet	92.1	94.7	82.9	88.8	80.4	87.8	90.0	78.5
ShelfNet	ResNet	92.1	94.8	84.1	88.9	78.0	87.6	90.1	77.9
MARsU-Net	ResNet	91.8	94.8	84.1	89.0	78.2	87.6	89.7	78.9
SwiftNet	ResNet	91.9	95.1	83.6	89.6	80.6	88.2	90.0	79.2
ABCNet	ResNet	93.1	94.8	84.8	90.0	84.7	89.5	91.2	81.0
BoTNet	ResNet	90.0	91.6	82.4	89.1	72.4	85.1	87.8	74.2
BANet	ResT-Lite	91.6	94.8	84.0	90.3	87.2	89.6	90.5	81.4
Segmenter	ViT-Tiny	90.1	92.6	80.7	90.3	68.2	84.4	87.6	73.7
UNetFormer	ResNet	93.1	94.9	85.2	90.8	88.2	90.4	90.7	83.2
GIB-RSS	-	94.7	96.8	86.8	89.9	91.5	91.8	92.9	85.3

dynamically adjust the LR. During model training, we use a random flip strategy for data augmentation. For the UAVid dataset, we crop the image size to 1024×1024 . For Vaihinge, Potsdam datasets, we crop images to 512×512 . When the GraphUNet is trained, we set epoch to 80, and batch size to 32.

C. Evaluation Metrics

We used multiple evaluation metrics to evaluate the experimental performance of all models, including Overall Accuracy (OA), meanF1, and mIoU. OA, F1 and mIOU reflect the

accuracy of remote sensing image segmentation from different angles.

D. Baseline models

MSD: The Multi-Scale-Dilation (MSD) method proposed by Lyu et al. [29] achieves image segmentation by using a large-scale pre-trained model to extract multi-scale features of the image.

CANet: The Context Aggregation Network (CANet) proposed by Yang et al. [32] effectively extracts the spatial information and global information of the image by building a

TABLE IV
EXPERIMENTAL RESULTS OF OUR METHOD AND SOTA LIGHTWEIGHT METHODS ON THE POTSDAM DATASET. THE OPTIMAL VALUES IN COLUMNS ARE SHOWN IN BOLD.

Methods	Backbone	Imp.suf.	Building	Lowveg.	Tree	Car	MeanF1	OA	mIoU
ERFNet	-	89.9	92.6	81.0	76.4	90.8	86.2	84.6	75.9
DABNet	-	90.0	92.7	83.3	81.9	93.1	88.0	87.2	79.4
BiSeNet	ResNet	90.2	94.6	85.5	86.2	92.7	89.8	88.2	81.7
EaNet	ResNet	92.0	95.7	84.3	85.7	95.1	90.6	88.7	83.4
MARsU-Net	ResNet	91.4	95.6	85.8	86.6	93.3	90.5	89.0	83.9
DANet	ResNet	91.0	95.6	86.1	87.6	84.3	88.9	89.1	80.3
SwiftNet	ResNet	91.8	95.9	85.7	86.8	94.5	91.0	89.3	83.8
FANet	ResNet	92.0	96.1	86.0	87.8	94.5	91.3	89.9	84.2
ShelfNet	ResNet	92.5	95.8	86.6	87.1	94.6	91.3	89.9	84.4
ABCNet	ResNet	93.5	96.9	87.9	89.1	95.8	92.7	91.3	86.5
Segmenter	ViT-Tiny	90.9	94.6	84.9	84.7	89.1	88.7	89.3	81.1
BANet	ResT-Lite	92.6	95.8	86.5	88.9	96.2	91.9	91.7	85.7
SwinUpperNet	Swin-Tiny	92.7	96.5	88.0	88.4	95.8	91.7	91.2	86.0
UNetFormer	ResNet	93.8	96.9	88.1	89.3	96.8	93.1	91.0	87.4
GIB-RSS	-	94.9	97.9	88.7	90.7	97.2	93.9	93.5	87.8

dual-branch CNN and uses an aggregation mechanism to fuse the spatial and global context information.

DANet: The dual attention network (DANet) proposed by Fu et al. [33] can achieve the extraction and fusion of global and local semantic information in space and channels.

SwiftNet: SwiftNet proposed by Orsic et al. [34] uses a pyramid structure to perform feature fusion of local information. SwiftNet adds regularization terms to constrain the model during the optimization process.

BiSeNet: The Bilateral Segmentation Network (BiSeNet) proposed by Yu et al. [35] extracts spatial information and high-resolution features by setting small-stride spatial convolution kernels. At the same time, a down-sampling strategy is used to extract contextual information, and a fusion module is designed to achieve effective fusion of information.

MANet: The multi-attention network (MANet) proposed by Li et al. [36] reduces the computational load of the model by building a linear attention module to ensure modeling context dependencies.

ABCNet: The Attention Bilateral Context Network (ABCNet) proposed by Li et al. [37] can lightweightly extract spatial information and contextual information of images.

Segmenter: Segmenter proposed by Strudel et al. [38] introduces ViT to realize the modeling of global context information. Unlike CNN, Segmenter can obtain class labels pixel by pixel.

SegFormer: SegFormer proposed by Xie et al. [39] combines Transformer and MLP to extract multi-scale features of images in a hierarchical manner.

BANet: Wang et al. [40] proposed a bilateral perception network (BANet) to extract texture information and boundary information in images in a fine-grained manner. BANet is based on the Transformer pre-training model to achieve information fusion.

BoTNet: The BoTNet proposed by Srinivas et al. [41] integrates the self-attention mechanism into the ResNet module to extract the global context information of the image.

TransUNet: TransUNet proposed by Chen et al. [42] embeds Transformer’s self-attention mechanism into the structure of UNet so that the model can better capture the global relationship of the input image.

ShelfNet: ShelfNet proposed by Zhuang et al. [43] adopts a multi-resolution processing strategy, which processes input images at different levels. Such a design allows the network to better capture local details in the image while retaining the global information of the image.

CoaT: CoaT proposed by Xu et al. [44] adopts a co-scaling mechanism to maintain the integrity of the Transformers encoder branch at different scales and provide rich multi-scale and contextual information.

UNetFormer: UNetFormer proposed by Wang et al. [45] introduces the Transformer mechanism based on UNet. In UNetFormer, Transformer is used to better capture the global contextual information in the image and improve the model’s ability to understand the overall structure.

V. RESULTS AND DISCUSSION

To illustrate the superiority of our proposed method GIB-RSS, we conduct experiments on four benchmark datasets (i.e., UAVid, Vaihingen, LoveDA, and Potsdam). The experimental results are shown in Tables II, III, IV, and V. GIB-RSS outperforms the existing state-of-the-art comparison algorithms.

Specifically, on the UAVid dataset as shown in Table II, GIB-RSS’s mIoU value is 70.6%, which is 3% to 11% higher than other models. The segmentation accuracy in other categories is also better than other comparison algorithms. For example, the IoU values of segmentation on cluster, road, tree, and vegetation have all reached SOTA, which is significantly

TABLE V
EXPERIMENTAL RESULTS OF OUR METHOD AND STATE-OF-THE-ART METHODS ON THE LOVEDA DATASET. THE OPTIMAL VALUES IN COLUMNS ARE SHOWN IN BOLD.

Methods	Backbone	Background	Building	Road	Water	Barren	Forest	Agriculture	mIoU	Complexity	Speed
PSPNet	ResNet50	44.4	52.1	53.5	76.5	9.7	44.1	57.9	48.3	105.7	52.2
DeepLabV3++	ResNet50	43.0	50.9	52.0	74.4	10.4	44.2	58.5	47.6	95.8	53.7
SemanticFPN	ResNet50	42.9	51.5	53.4	74.7	11.2	44.6	58.7	48.2	103.3	52.7
FarSeg	ResNet50	43.1	51.5	53.9	76.6	9.8	43.3	58.9	48.2	-	47.8
FactSeg	ResNet50	42.6	53.6	52.8	76.9	16.2	42.9	57.5	48.9	-	46.7
BANet	ResNet50	43.7	51.5	51.1	76.9	16.6	44.9	62.5	49.6	52.6	11.5
TransUNet	ViT-R50	43.0	56.1	53.7	78.0	9.3	44.9	56.9	48.9	803.4	13.4
Segmenter	ViT-Tiny	38.0	50.7	48.7	77.4	13.3	43.5	58.2	47.1	26.8	14.7
SwinUpperNet	Swin-Tiny	43.3	54.3	54.3	78.7	14.9	45.3	59.6	50.0	349.1	19.5
DC-Swin	Swin-Tiny	41.3	54.5	56.2	78.1	14.5	47.2	62.4	50.6	183.8	23.6
UNetFormer	ResNet18	44.7	58.8	54.9	79.6	20.1	46.0	62.5	52.4	46.9	115.3
GIB-RSS	-	45.8	59.6	56.4	80.4	21.2	48.2	63.7	54.1	34.2	122.1

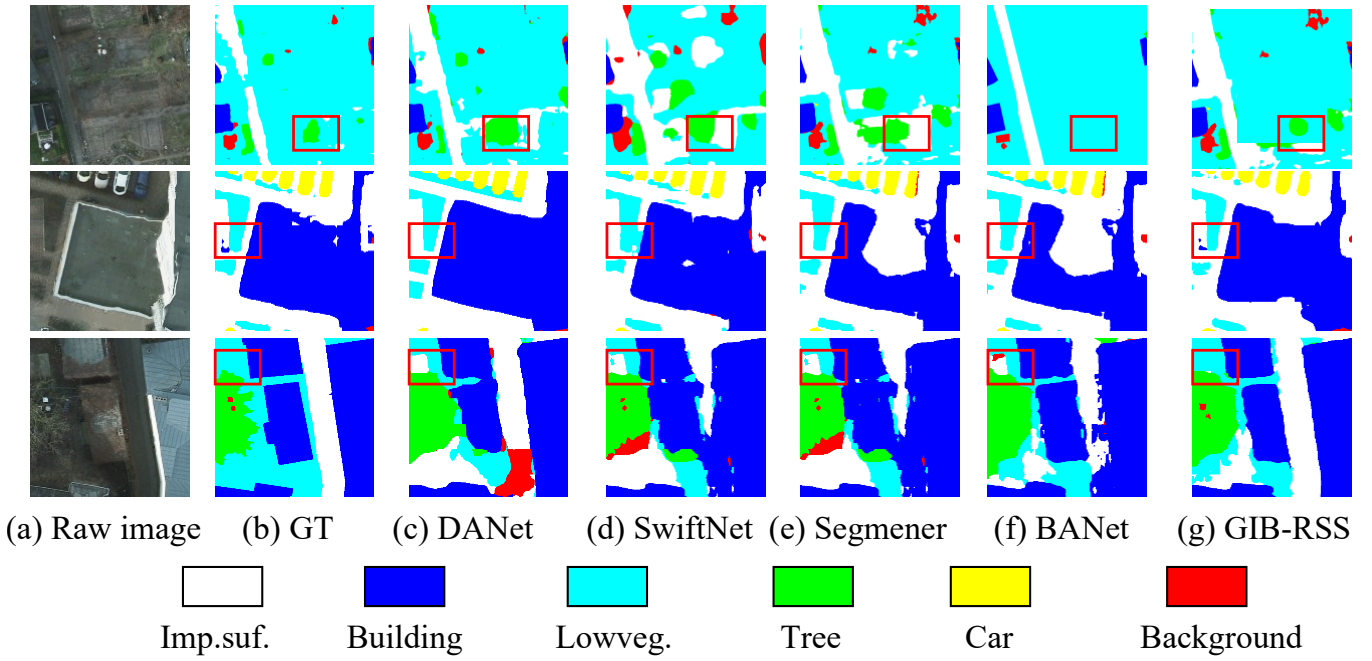


Fig. 4. Visualization of the segmentation results of different models on the Postdam dataset.

better than existing methods. Although the IoU values on building, movingcar and human are not optimal, the difference from the best segmentation results is relatively small. Among other comparison algorithms, UNetFormer’s effect is slightly lower than our algorithm, with an mIoU value of 67.8%. We believe this is due to the fact that the architecture we designed is more suitable for segmenting irregular objects. Except for UNetFormer, the mIoU values of other comparison algorithms are significantly lower than the method GIB-RSS proposed in this paper.

On the Vaihingen dataset as shown in Table III, GSIB-RSS’s mIoU value is 85.3%, which is 2% to 6% higher than other models. OA and meanF1 values are also higher than other methods. Specifically, the segmentation IoU value of our

method GIB-RSS in four categories is significantly better than that of other comparison algorithms. It is only lower than some comparison algorithms (e.g., UNetFormer and segmenter, etc.) in the tree category. The effect of UNetFormer is second, its mIoU value is 67.8%, which is 1.8% lower than GIB-RSS. The segmentation effects of other comparison algorithms are significantly lower than GIB-RSS and UNetFormer, even if they use some pre-trained models with better performance.

On the Potsdam dataset as shown in IV, GIB-RSS’s mIoU value is 87.8%, which is 1% to 12% higher than other models. Our algorithm GIB-RSS is significantly better than other comparison algorithms in the segmentation effects of all categories. Similarly, UNetFormer has the second best segmentation effect on the Potsdam dataset, with an mIoU

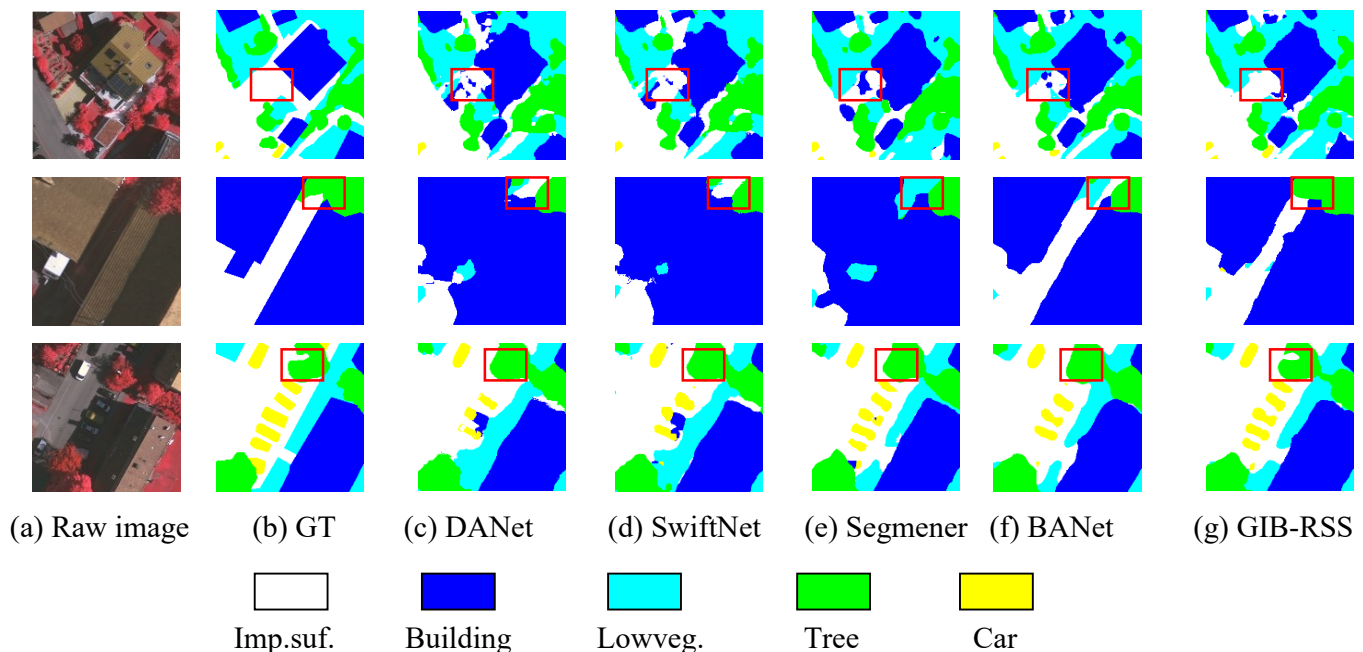


Fig. 5. Visualization of the segmentation results of different models on the Vaihingen dataset.

value of 87.4%. Other comparison algorithms usually use pre-trained models such as ResNet or ViT as backbone to fine-tune downstream tasks. Although the segmentation effect on the Potsdam data set is okay, it is lower than GIB-RSS.

On the LoveDA dataset as shown in V, GIB-RSS can achieve optimal segmentation results in all categories. In addition, GIB-RSS has a model parameter volume of 34.2M and an inference speed of 122.1fps, which is far superior to other comparison algorithms. Like other comparison algorithms, due to the use of large-scale pre-training models, this results in a relatively large number of model parameters and slow inference speed.

The performance improvement may be attributed to our method’s ability to flexibly model irregular objects, and the introduction of the multi-head attention effectively improves the model’s capture of key position information in the image. At the same time, we also introduced the information bottleneck theory to perform graph comparison learning. Unlike the previous GCL method, GIB obtains optimal graph structure representation by minimizing the mutual information between nodes. The intuition behind this is that a good augmented multi-view should be structurally heterogeneous but semantically similar. However, the existing methods are all based on CNN or Transformer architecture, and their ability to extract global position information of irregular objects is worse than GNN.

VI. VISUALIZATION OF SEGMENTATION RESULTS

As shown in Figs. 4, 5, and 6, we also intuitively display the segmentation results of the model. The visualized segmentation results demonstrate the effectiveness of our designed GIB-RSS in dealing with challenging irregular objects.

Specifically, in Fig. 4, we see that GIB-RSS can more accurately segment trees and buildings than other SOTA

models, and the cases of wrong segmentation are relatively small. Other models easily misclassify lowveg. categories as background categories, and they fail to learn better for building category boundaries. In particular, in the first row of images, existing methods cannot segment the tree category well, either identifying it as background or identifying it as other categories. In the second row of pictures, existing comparison methods cannot segment some relatively small categories well, while GIB-RSS can segment small irregular objects better. In the third row of images, GIB-RSS can better segment the boundary areas of two different categories.

As shown in Fig. 5, our proposed model is more clearly distinguish the difference between trees and lowveg. The experimental results show that GIB-RSS more effectively learn the boundary information between different categories. The class boundary learning ability of other models is significantly worse than GIB-RSS. Specifically, in the first row of images, our method can better identify the background area, while other comparison methods easily misclassify the background area as a building category. In the second row of pictures, GIB-RSS can segment the tree category relatively completely, while other methods easily identify the tree category as a background category or other categories. In the third row of images, GIB-RSS can sensitively detect the boundary areas of categories, while other methods cannot correctly segment the boundary areas of categories.

As shown in Fig. 6, in the first row of images, existing methods cannot correctly classify the tree category, but incorrectly classify it as the agriculture category. Unlike contrastive methods, GIB-RSS can well distinguish the difference between two categories and achieve better class boundary segmentation. In the second row of pictures, since the segmented objects are relatively small, existing methods cannot perform fine-grained segmentation on them. GIB-RSS can segment small objects at

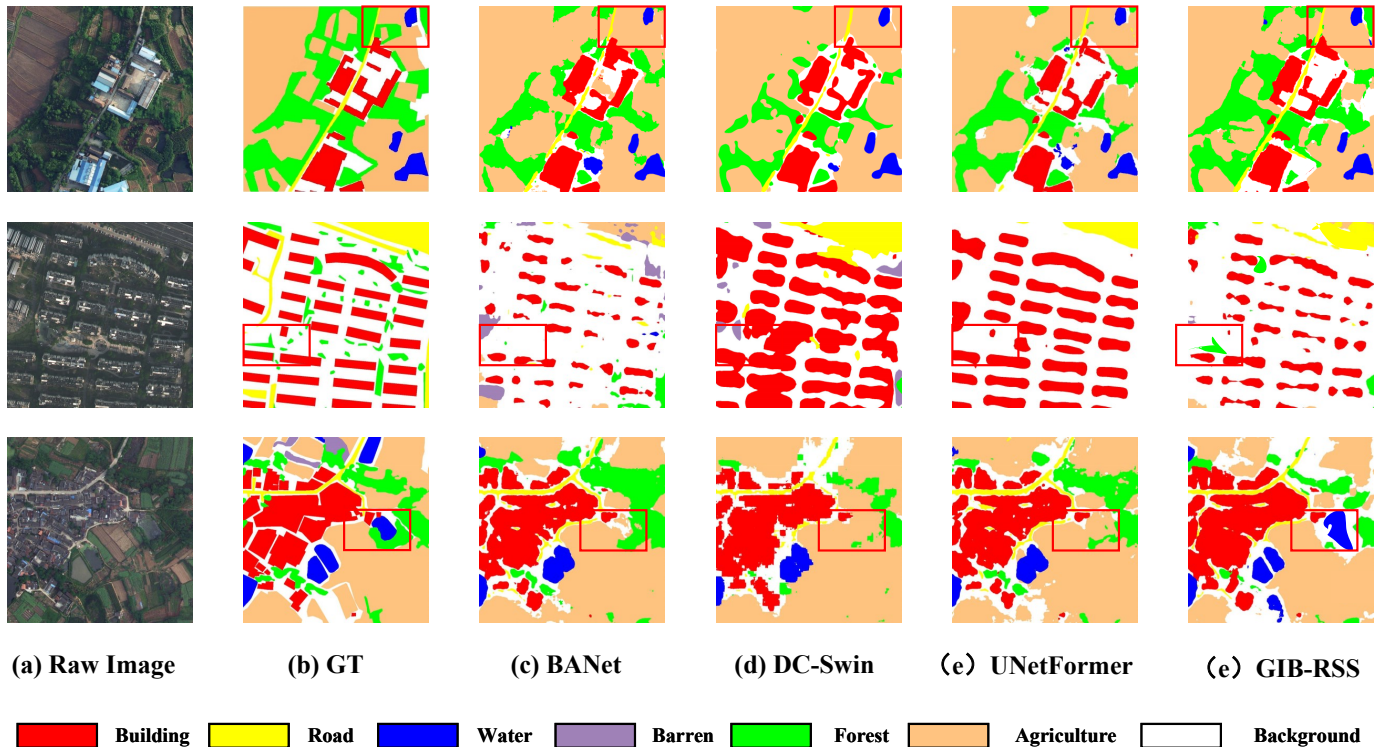


Fig. 6. Visualization of the segmentation results of different models on the LoveDA dataset.

fine granularity while also distinguishing differences between tree and background categories. In the third row of images, none of the existing comparison methods can segment the water category, while GIB-RSS can segment them accurately. Experimental results demonstrate the superior segmentation performance of the GIB method for irregular objects.

VII. ABLATION STUDY

We conduct ablation studies of our model GIB-RSS on four segmentation datasets to illustrate the effectiveness of our used modules.

TABLE VI
EXPERIMENTAL RESULTS OF DIFFERENT TYPES OF GRAPH CONVOLUTIONAL NEURAL NETWORKS ON DATASETS. WE CHOOSE THE mIOU VALUE AS OUR EVALUATION METRIC.

GraphConv	UAVid	Vaihingen	Potsdam	LoveDA
EdgeConv	69.5	84.4	86.9	53.6
GIN	68.7	83.6	86.7	53.1
GraphSAGE	68.6	83.4	86.2	52.7
GAT	70.6	85.3	87.8	54.1

A. Type of graph convolution

In experiments we explore the performance of three different graph convolution variants on segmentation, including EdgeConv, GIN, GraphSAGE, and GAT. As shown in Table VI, GAT achieves the highest accuracy with mIoU values of

79.6%, 85.3%, 87.8% and 54.1% on the four datasets. The effect of EdgeConv is second, with mIoU values of 69.5%, 84.4%, 86.9% and 53.6% on the four datasets. The effect of GraSAGE is worst, with mIoU values of 68.6%, 83.4%, 86.2% and 52.7% on the four datasets. The performance improvement may be attributed to GAT’s ability to capture key region information in the image.

B. The effects of modules in GIB-RSS

To illustrate that the modules (i.e., node-masking and edge-masking) proposed in this paper can better improve the performance of GNN in the field of image segmentation, we verify the effect of these modules through ablation studies. We use node mask view and edge mask view with information bottleneck criterion to improve the generalization ability of the model. From Table VII we can see that the performance of image segmentation using graph convolution alone is not competitive. The accuracy of segmentation can be improved by introducing node-masking and edge-masking. Specifically, the model performs best when using both node mask and edge mask views, with mIoU values of 70.6%, 85.3%, 87.8% and 54.1% respectively. When only using the node mask view, the effect of the model is second, with mIoU values of 68.2%, 82.3%, 86.5% and 53.8% respectively. The model has the worst performance when the node mask and edge mask views are not used, with mIoU values of 67.5%, 81.8%, 86.2% and 53.0% respectively.

C. The number of neighbors

The number of neighbor nodes K is a hyperparameter controlling information aggregation. Too few neighbor nodes

TABLE VII

THE EFFECTIVENESS OF THE PROPOSED THREE CORE MODULES (I.E., FFN, MULTI HEADS, AND GRAPHCONV) IS VERIFIED BY ABLATION EXPERIMENTS ON THE DATASET. WE CHOOSE THE MIOU VALUE AS OUR EVALUATION METRIC.

GraphConv	Node-masking	Edge-masking	UAVid	Vaihingen	Potsdam	LoveDA
✓	✗	✗	67.5	81.8	86.2	53.0
✓	✓	✗	68.0	81.7	85.4	53.6
✓	✗	✓	68.2	82.3	86.5	53.8
✓	✓	✓	70.6	85.3	87.8	54.1

will lead to low frequency of information exchange, and the global position information cannot be fully extracted, while too many neighbors will lead to over-smoothing of the model. Based on the above analysis, we adjusted the range of K from 3 to 18, and the results are shown in Table VIII. When the number of neighbor nodes K is 15, the segmentation effect is better. When the number of nodes K is less than 15, the effect of the model increases as the number of K increases, and when K is greater than 15, the training effect of the model begins to show a downward trend. The above phenomenon is consistent with our analysis.

TABLE VIII

THE INFLUENCE OF DIFFERENT NUMBER OF NEIGHBOR NODES K ON THE EXPERIMENTAL RESULTS. WE CHOOSE THE MIOU VALUE AS OUR EVALUATION METRIC.

K	UAVid	Vaihingen	Potsdam	LoveDA
3	66.7	82.5	84.4	52.1
6	67.6	82.9	85.8	52.7
9	67.8	83.3	85.9	52.9
12	68.9	84.2	86.6	53.6
15	70.6	85.3	87.8	54.1
18	69.3	83.9	87.0	53.6

VIII. CONCLUSIONS

In this paper, we regard images as graph data and introduce GNN to perform remote sensing image segmentation tasks, which can flexibly model irregular objects. To extract the global contextual location information in the image, we introduce a multi-head attention mechanism for global information extraction. Furthermore, we introduce a feed-forward network for each node to perform feature transformation on node features to encourage information diversity. In addition, in order to accelerate the convergence speed of GNN, we introduce the information bottleneck theory for graph comparison learning. We argue that a good augmented view should be structurally heterogeneous but semantically similar. Experimental results prove the superiority of our model GIB-RSS.

In the follow-up research, We hope to introduce some large-scale pre-trained models to achieve zero-shot image segmentation.

REFERENCES

- [1] Y. Shou, T. Meng, W. Ai, C. Xie, H. Liu, and Y. Wang, "Object detection in medical images based on hierarchical transformer and mask mechanism," *Computational Intelligence and Neuroscience*, vol. 2022, 2022.
- [2] N. Yin, L. Shen, M. Wang, X. Luo, Z. Luo, and D. Tao, "Omg: Towards effective graph classification against label noise," *IEEE Transactions on Knowledge and Data Engineering*, vol. 35, no. 12, pp. 12 873–12 886, 2023.
- [3] N. Yin, L. Shen, H. Xiong, B. Gu, C. Chen, X. Hua, S. Liu, and X. Luo, "Messages are never propagated alone: Collaborative hypergraph neural network for time-series forecasting," *IEEE Transactions on Pattern Analysis and Machine Intelligence*, no. 01, pp. 1–15, nov 5555.
- [4] N. Yin, L. Shen, M. Wang, L. Lan, Z. Ma, C. Chen, X.-S. Hua, and X. Luo, "Coco: A coupled contrastive framework for unsupervised domain adaptive graph classification," *arXiv preprint arXiv:2306.04979*, 2023.
- [5] N. Yin, L. Shen, B. Li, M. Wang, X. Luo, C. Chen, Z. Luo, and X.-S. Hua, "Deal: An unsupervised domain adaptive framework for graph-level classification," in *Proceedings of the 30th ACM International Conference on Multimedia*, ser. MM '22. New York, NY, USA: Association for Computing Machinery, 2022, p. 3470–3479.
- [6] Y. Shou, T. Meng, W. Ai, S. Yang, and K. Li, "Conversational emotion recognition studies based on graph convolutional neural networks and a dependent syntactic analysis," *Neurocomputing*, vol. 501, pp. 629–639, 2022.
- [7] J. Long, E. Shelhamer, and T. Darrell, "Fully convolutional networks for semantic segmentation," in *Proceedings of the IEEE Conference on Computer Vision and Pattern Recognition*, 2015, pp. 3431–3440.
- [8] S. Wu, J. Shi, and Z. Chen, "Hg-fcn: Hierarchical grid fully convolutional network for fast vvc intra coding," *IEEE Transactions on Circuits and Systems for Video Technology*, vol. 32, no. 8, pp. 5638–5649, 2022.
- [9] Z. Zhou, M. M. Rahman Siddiquee, N. Tajbakhsh, and J. Liang, "Unet++: A nested u-net architecture for medical image segmentation," in *Deep Learning in Medical Image Analysis and Multimodal Learning for Clinical Decision Support: 4th International Workshop, DLMIA 2018, and 8th International Workshop, ML-CDS 2018, Held in Conjunction with MICCAI 2018, Granada, Spain, September 20, 2018, Proceedings 4*. Springer, 2018, pp. 3–11.
- [10] H. Cao, Y. Wang, J. Chen, D. Jiang, X. Zhang, Q. Tian, and M. Wang, "Swin-unet: Unet-like pure transformer for medical image segmentation," in *European conference on computer vision*. Springer, 2022, pp. 205–218.
- [11] C. Liang-Chieh, G. Papandreou, I. Kokkinos, K. Murphy, and A. Yuille, "Semantic image segmentation with deep convolutional nets and fully connected crfs," in *International Conference on Learning Representations*, 2015.
- [12] J. Wang, K. Sun, T. Cheng, B. Jiang, C. Deng, Y. Zhao, D. Liu, Y. Mu, M. Tan, X. Wang *et al.*, "Deep high-resolution representation learning for visual recognition," *IEEE transactions on pattern analysis and machine intelligence*, vol. 43, no. 10, pp. 3349–3364, 2020.
- [13] A. Vaswani, N. Shazeer, N. Parmar, J. Uszkoreit, L. Jones, A. N. Gomez, E. Kaiser, and I. Polosukhin, "Attention is all you need," *Advances in neural information processing systems*, vol. 30, 2017.
- [14] A. Dosovitskiy, L. Beyer, A. Kolesnikov, D. Weissenborn, X. Zhai, T. Unterthiner, M. Dehghani, M. Minderer, G. Heigold, S. Gelly *et al.*, "An image is worth 16x16 words: Transformers for image recognition at scale," in *International Conference on Learning Representations*, 2020.
- [15] Z. Liu, Y. Lin, Y. Cao, H. Hu, Y. Wei, Z. Zhang, S. Lin, and B. Guo, "Swin transformer: Hierarchical vision transformer using shifted windows," in *Proceedings of the IEEE/CVF International Conference on Computer Vision*, 2021, pp. 10012–10022.
- [16] L. Ding, D. Lin, S. Lin, J. Zhang, X. Cui, Y. Wang, H. Tang, and L. Bruzzone, "Looking outside the window: Wide-context transformer for the semantic segmentation of high-resolution remote sensing images," *IEEE Transactions on Geoscience and Remote Sensing*, vol. 60, pp. 1–13, 2022.
- [17] C. Zhang, W. Jiang, Y. Zhang, W. Wang, Q. Zhao, and C. Wang, "Transformer and cnn hybrid deep neural network for semantic segmentation of very-high-resolution remote sensing imagery," *IEEE Transactions on Geoscience and Remote Sensing*, vol. 60, pp. 1–20, 2022.
- [18] T. N. Kipf and M. Welling, "Semi-supervised classification with graph convolutional networks," *arXiv preprint arXiv:1609.02907*, 2016.
- [19] Y. Mo, L. Peng, J. Xu, X. Shi, and X. Zhu, "Simple unsupervised graph representation learning," in *Proceedings of the AAAI Conference on Artificial Intelligence*, vol. 36, no. 7, 2022, pp. 7797–7805.

- [20] Z. Wen and Y. Fang, "Trend: Temporal event and node dynamics for graph representation learning," in *Proceedings of the ACM Web Conference 2022*, 2022, pp. 1159–1169.
- [21] X. Hao, J. Li, Y. Guo, T. Jiang, and M. Yu, "Hypergraph neural network for skeleton-based action recognition," *IEEE Transactions on Image Processing*, vol. 30, pp. 2263–2275, 2021.
- [22] W. Shi and R. Rajkumar, "Point-gnn: Graph neural network for 3d object detection in a point cloud," in *Proceedings of the IEEE/CVF conference on computer vision and pattern recognition*, 2020, pp. 1711–1719.
- [23] K. Han, Y. Wang, J. Guo, Y. Tang, and E. Wu, "Vision gnn: An image is worth graph of nodes," *Advances in Neural Information Processing Systems*, vol. 35, pp. 8291–8303, 2022.
- [24] S. Saha, S. Zhao, and X. X. Zhu, "Multitarget domain adaptation for remote sensing classification using graph neural network," *IEEE Geoscience and Remote Sensing Letters*, vol. 19, pp. 1–5, 2022.
- [25] P. Veličković, W. Fedus, W. L. Hamilton, P. Liò, Y. Bengio, and R. D. Hjelm, "Deep graph infomax," in *International Conference on Learning Representations*, 2018.
- [26] F.-Y. Sun, J. Hoffman, V. Verma, and J. Tang, "Infograph: Unsupervised and semi-supervised graph-level representation learning via mutual information maximization," in *International Conference on Learning Representations*, 2019.
- [27] K. Hassani and A. H. Khasahmadi, "Contrastive multi-view representation learning on graphs," in *International conference on machine learning*. PMLR, 2020, pp. 4116–4126.
- [28] Y. You, T. Chen, Y. Sui, T. Chen, Z. Wang, and Y. Shen, "Graph contrastive learning with augmentations," *Advances in neural information processing systems*, vol. 33, pp. 5812–5823, 2020.
- [29] Y. Lyu, G. Vosselman, G.-S. Xia, A. Yilmaz, and M. Y. Yang, "Uavid: A semantic segmentation dataset for uav imagery," *ISPRS journal of photogrammetry and remote sensing*, vol. 165, pp. 108–119, 2020.
- [30] H. Li, K. Qiu, L. Chen, X. Mei, L. Hong, and C. Tao, "Scattnet: Semantic segmentation network with spatial and channel attention mechanism for high-resolution remote sensing images," *IEEE Geoscience and Remote Sensing Letters*, vol. 18, no. 5, pp. 905–909, 2020.
- [31] A. Boguszewski, D. Batorski, N. Ziemia-Jankowska, T. Dzedzic, and A. Zambrzycka, "Landcover. ai: Dataset for automatic mapping of buildings, woodlands, water and roads from aerial imagery," in *Proceedings of the IEEE/CVF Conference on Computer Vision and Pattern Recognition*, 2021, pp. 1102–1110.
- [32] M. Y. Yang, S. Kumaar, Y. Lyu, and F. Nex, "Real-time semantic segmentation with context aggregation network," *ISPRS journal of photogrammetry and remote sensing*, vol. 178, pp. 124–134, 2021.
- [33] J. Fu, J. Liu, H. Tian, Y. Li, Y. Bao, Z. Fang, and H. Lu, "Dual attention network for scene segmentation," in *Proceedings of the IEEE/CVF Conference on Computer Vision and Pattern Recognition*, 2019, pp. 3146–3154.
- [34] M. Oršić and S. Šegvić, "Efficient semantic segmentation with pyramidal fusion," *Pattern Recognition*, vol. 110, p. 107611, 2021.
- [35] C. Yu, J. Wang, C. Peng, C. Gao, G. Yu, and N. Sang, "Bisenet: Bilateral segmentation network for real-time semantic segmentation," in *Proceedings of the European conference on computer vision (ECCV)*, 2018, pp. 325–341.
- [36] R. Li, S. Zheng, C. Zhang, C. Duan, J. Su, L. Wang, and P. M. Atkinson, "Multiattention network for semantic segmentation of fine-resolution remote sensing images," *IEEE Transactions on Geoscience and Remote Sensing*, vol. 60, pp. 1–13, 2021.
- [37] R. Li, S. Zheng, C. Zhang, C. Duan, L. Wang, and P. M. Atkinson, "Abcnnet: Attentive bilateral contextual network for efficient semantic segmentation of fine-resolution remotely sensed imagery," *ISPRS journal of photogrammetry and remote sensing*, vol. 181, pp. 84–98, 2021.
- [38] R. Strudel, R. Garcia, I. Laptev, and C. Schmid, "Segmenter: Transformer for semantic segmentation," in *Proceedings of the IEEE/CVF international conference on computer vision*, 2021, pp. 7262–7272.
- [39] E. Xie, W. Wang, Z. Yu, A. Anandkumar, J. M. Alvarez, and P. Luo, "Segformer: Simple and efficient design for semantic segmentation with transformers," *Advances in Neural Information Processing Systems*, vol. 34, pp. 12077–12090, 2021.
- [40] L. Wang, R. Li, D. Wang, C. Duan, T. Wang, and X. Meng, "Transformer meets convolution: A bilateral awareness network for semantic segmentation of very fine resolution urban scene images," *Remote Sensing*, vol. 13, no. 16, p. 3065, 2021.
- [41] A. Srinivas, T.-Y. Lin, N. Parmar, J. Shlens, P. Abbeel, and A. Vaswani, "Bottleneck transformers for visual recognition," in *Proceedings of the IEEE/CVF conference on computer vision and pattern recognition*, 2021, pp. 16519–16529.
- [42] J. Chen, Y. Lu, Q. Yu, X. Luo, E. Adeli, Y. Wang, L. Lu, A. L. Yuille, and Y. Zhou, "Transunet: Transformers make strong encoders for medical image segmentation," *arXiv preprint arXiv:2102.04306*, 2021.
- [43] J. Zhuang, J. Yang, L. Gu, and N. Dvornek, "Shelfnet for fast semantic segmentation," in *Proceedings of the IEEE/CVF international conference on computer vision workshops*, 2019, pp. 0–0.
- [44] W. Xu, Y. Xu, T. Chang, and Z. Tu, "Co-scale conv-attentional image transformers," in *Proceedings of the IEEE/CVF International Conference on Computer Vision*, 2021, pp. 9981–9990.
- [45] L. Wang, R. Li, C. Zhang, S. Fang, C. Duan, X. Meng, and P. M. Atkinson, "Unetformer: A unet-like transformer for efficient semantic segmentation of remote sensing urban scene imagery," *ISPRS Journal of Photogrammetry and Remote Sensing*, vol. 190, pp. 196–214, 2022.